

Physiological tradeoffs in the parameterization of a model of canopy transpiration

D.S. Mackay^{a,b,*}, D.E. Ahl^b, B.E. Ewers^a, S. Samanta^a, S.T. Gower^a, S.N. Burrows^a

^a Department of Forest Ecology and Management, Institute for Environmental Studies, University of Wisconsin-Madison, 1630 Linden Dr., Madison, WI 53706, USA

^b Environmental Remote Sensing Center, Institute for Environmental Studies, 1225 West Dayton St., WI 53715, USA

Abstract

We examined physiological parameter tradeoffs in modeling stomatal control of transpiration from a number of forest species. Measurements of sapflux, micrometeorology, and leaf area index were made in stands representing 85% of the forest ecosystems around the WLEF eddy flux tower in northern Wisconsin. A Jarvis-based canopy conductance model was used to simulate canopy transpiration (E_C) for five tree species from these stands. They consisted of conifers and deciduous species in both upland and wetland locations. Parameter estimation was used to assess the tradeoffs between physiological parameters used in the calculation of stomatal conductance. These tradeoffs were then evaluated against current theory on stomatal regulation of leaf water potential. The results show that the best simulations of E_C were obtained with values of maximum stomatal conductance (g_{Smax}) and stomatal sensitivity to vapor pressure deficit (δ) that closely followed this hydraulic theory. The model predictions reveal a large variation in the strategies used to regulate water potential among species. Aspen showed the greatest tendency towards efficiency, indicating that it has high E_C under low vapor pressure deficit (D) conditions, but is susceptible to rapid E_C decline at moderate to high D . Other species showed more conservative water use. The results indicate that inter-specific differences in dynamic response to D can produce large spatial variation in E_C under typical environmental conditions.

© 2002 Elsevier Science Ltd. All rights reserved.

Keywords: Canopy conductance; Canopy transpiration; Forest water fluxes; Land surface process modeling; Parameter estimation; TREES

1. Introduction

Spatially variable canopy transpiration is a major component in distributed simulation models of land surface processes. There is currently very little observational data to directly support large-scale simulation of canopy transpiration from forests. Nevertheless, many large-scale models operating at watershed, regional and global scale [1,3,6,19,24,25,46,57,59,63,72,73] [others] simulate transpiration using some form of the Penman–Monteith (P–M) combination equation [49] and one of several empirical models of stomatal conductance [5,34,43]. Assuming that these models correctly describe the biophysical mechanisms (or surrogates) of transpiration, a major task for land surface modelers is

to develop and apply indirect methods to improve model parameterization. The data needed for this parameterization can come from in situ monitoring and/or remote sensing techniques. In situ flux measurements can be used to improve estimates of model parameters [9,31,67], but these may be difficult to apply spatially [8]. The parameters obtained in the process of matching model results to measurements may be too specific to the data used. Remote sensing data can provide important proxy information for conditioning parameter selection on spatial variables [26,27,52,56], and for testing spatially distributed mechanisms in models of forest water fluxes [44]. In situ measurements are essential for improving and testing process models.

In this paper, in situ measurements of sap flux and micrometeorological variables are used to parameterize the stomatal physiology of a model of canopy transpiration applied to several forest stands with multiple tree species. The motivating question for this paper is, to what extent can physiologically meaningful parameter values be resolved in the process of simulating stomatal

* Corresponding author. Address: Department of Forest Ecology and Management, Institute for Environmental Studies, University of Wisconsin-Madison, 1630 Linden Dr., Madison, WI 53706, USA. Tel.: +1-608-262-1669; fax: +1-608-262-9922.

E-mail address: dsmackay@facstaff.wisc.edu (D.S. Mackay).

conductance for estimating daily transpiration? If parameter estimates are to be reliably applied beyond individual forest stands, then it is important that interspecies differences in parameter values be directly related to differences in stomatal physiology. By accounting for these differences, then more reliable surface resistance parameterizations may be realized in heterogeneous forested landscapes.

The widely used P–M model of canopy transpiration has the form:

$$E_C = \frac{\Delta R_n + C_p \rho_a \frac{D}{r_a}}{\rho_w \lambda \left(\Delta + \gamma \left(1 + \frac{r_c}{r_a} \right) \right)}, \quad (1)$$

where E_C is canopy transpiration (m s^{-1}), Δ is the slope of the saturation vapor pressure–temperature curve ($\text{mbar } ^\circ\text{C}^{-1}$), R_n is canopy net radiation (W m^{-2}), C_p is specific heat capacity of air ($\text{J kg}^{-1} ^\circ\text{C}^{-1}$), ρ_a is the density of air (kg m^{-3}), D is vapor pressure deficit from canopy to air (mbar), r_a is the bulk vegetation aerodynamic resistance (s m^{-1}), ρ_w is the density of water (kg m^{-3}), λ is the latent heat of evaporation (J kg^{-1}), γ is the psychrometric constant ($\text{mbar } ^\circ\text{C}^{-1}$), and r_c is canopy resistance (s m^{-1}). Aerodynamic resistance, r_a , is affected by canopy properties and the flow of air through and above the canopy. Canopy resistance, r_c , is affected by the environmental (extrinsic) and physiological (intrinsic) conditions of the leaf stomata. There are two distinct approaches to building models of stomatal conductance: Ball–Berry [5,42] and Jarvis [34,43]. Ball–Berry models have the form:

$$g_S = m[(A_n h_S / c_S)] + b, \quad (2)$$

where m and b are empirical constants, A_n is net photosynthetic rate, h_S is relative humidity at the leaf surface, and c_S is CO_2 mole fraction at the leaf surface. Ball–Berry models do a good job of estimating carbon assimilation by explicitly accounting for the coupled assimilation–conductance response using biochemical models [20,21] parameterized by species [74]. Jarvis-type models have the general form:

$$g_S = g_{S_{\max}} \cdot \prod f_i, \quad (3)$$

where $g_{S_{\max}}$ is a theoretical maximum stomatal conductance under optimal environmental and leaf conditions. A series of functions of environmental factors (f_i) are applied to reduce actual leaf level stomatal conductance from the optimal level. For instance, one function considers the stomatal sensitivity, δ , to D . The $g_{S_{\max}}$ parameter can vary widely among and within species [38,17] and δ is widely believed to increase with $g_{S_{\max}}$ [34,35,48,50,53,61]. When vapor pressure gradients are low, the conditions favor stomatal control by assimilation rate, but as D increases stomata close to reduce water loss [5,50,61,75]. The advantage of the Jarvis

model for hydrologic processes is that it directly addresses plant response to D , which means it works best when the rate of water loss is high and hence hydrologically significant. Furthermore, recent developments in plant hydraulic theory have been successfully combined with Jarvis models [18,53].

Eq. (3) and its parameters are surrogates for processes occurring throughout the soil–plant atmosphere continuum. In the absence of stomatal control, a high rate of water loss can lead to a rapid decline in leaf water potential, which increases the risk of hydraulic failure in the plant [18,53,68]. This can be expressed in terms of a supply function through the soil–plant continuum, which has been derived from the steady-state assumption and Darcy’s law [18,68,69]:

$$G_S = K_L / D(\Psi_S - \Psi_L - h\rho_w g), \quad (4)$$

where G_S is canopy average stomatal conductance, K_L is leaf-specific hydraulic conductance, Ψ_S and Ψ_L are bulk soil and leaf water potentials, and $h\rho_w g$ is the gravitational potential for a tree of height h . K_L declines with water potential due to soil drying, cavitation in the xylem, and other factors. This results in a feedback on water loss, because the water potential needed to sustain increasing E_C per unit leaf area (L) produces a decline in K_L . If the maximum safe transpiration rate is exceeded then runaway cavitation ensues. This refers to K_L being driven to zero causing hydraulic failure and possible plant mortality [70]. Eq. (4) also captures the well-known fact that G_S is inversely proportional to D [34,48]. Furthermore, G_S is sensitive to increasing D in proportion to some maximum conductance, $g_{S_{\max}}$, or its proxy [53]:

$$G_S = G_{S_{\text{ref}}} - m \cdot \ln D, \quad (5)$$

where $G_{S_{\text{ref}}}$ is a substitute for $g_{S_{\max}}$ defined at $D = 1$ kPa and $m = dG_S/d \ln D$ is the sensitivity of stomatal conductance to increasing D . The chosen form of Eq. (5) provides a linear relationship between the reference conductance and sensitivity of stomatal conductance to D . Based on a large amount of porometry and sap flux data, Oren et al. [53] have shown that $m \approx 0.6 G_{S_{\text{ref}}}$ applies universally to all species that regulate leaf water potential to just prevent runaway cavitation.

The goal of this paper is to assess whether a canopy model based on the Jarvis approach can be meaningfully parameterized to capture the stomatal regulation of leaf water potential such that it obeys the hydraulic theory presented above. We begin by introducing a diurnal land surface process model and a method of automated parameter estimation to generate sets of physiologically acceptable model–parameter combinations among a number of dominant forest species in northern Wisconsin. We first determine consistent parameter values from a fuzzy logic approach, calibrate the model against transpiration estimated with sap flux from five tree

species to find optimal sets of parameter values, and then analyze these best sets to detect physiological tradeoffs and differences among tree species. The physiological tradeoffs are described in terms of current understanding in plant–water relations, as a theoretical framework for improving the scalability of species-based transpiration models for incorporation into large-scale land surface models of heterogeneous forests.

2. Methods

2.1. Site description

The study was conducted in northern Wisconsin, near Park Falls (45.94 °N, 90.27 °W). The study area is a 12-km² region centered on a 447-m tall communications tower (WLEF tower) instrumented to measure energy, water and carbon exchange between the forest landscape and the atmosphere [4]. The tower and surrounding area is located in the Chequamegon-Nicolet National Forest. The area is situated in the Northern Highlands physiographic province, a southern extension of the Canadian Shield. The bedrock is comprised of Precambrian metamorphic and igneous rock overlain by 8–90 m of glacial and glaciofluvial material. The topography is slightly rolling with a range of 45 m. The growing season is short and the winters are long and cold. Mean annual July and January temperatures are 19 and –12 °C, respectively.

The forested vegetation reflects the glacial topography [22,23] and history of forest management activities [11]. Red pine (*Pinus resinosa* Ait) and Jack pine (*Pinus banksiana* Lamb) dominate areas of excessively drained glacial outwash. Northern hardwood forests, comprised of sugar maple (*Acer saccharum* Marsh), red maple (*Acer rubrum* L.), green ash (*Fraxinus americana*), yellow birch (*Betula alleghaniensis* Britton) and basswood (*Tilia americana* L.), occur on the finer textured moraines and drumlins. Intermediate sites support a wide variety of broad-leaf deciduous tree species, such as quaking aspen (*Populus tremuloides* Michx), bigtooth aspen (*Populus grandidentata* Michx), paper birch (*Betula papyrifera* Marsh), red maple, and red and white pine (*Pinus strobus*). Poorly drained lowland sites are dominated by white cedar (*Thuja occidentalis* L.), balsam fir (*Abies balsamea*(L.) Mill), white spruce (*Picea glauca*), black spruce (*Picea mariana*), tamarack (*Larix laricina*), and speckled alder (*Alnus regosa*). Within the study area leaf area, L , during summer of year 2000, averaged 3.6 m² m⁻². Most of the forests had L values in the range of 3.5–4.0 m² m⁻² [11].

2.2. Stand-level measurements

Five primary species were selected for intensive study including red pine, sugar maple, trembling aspen, white

cedar, and speckled alder. These species represent over 80% of the tree basal area [11] and about 85% of land surface area [45] around the WLEF tower. The average LAI for each stand was 3.6 m² m⁻² and did not change significantly throughout the measurement period [15]. Granier-type sap flux sensors [30] were used to record sap flow in the hydroactive xylem of selected trees in each stand. Sap flux measurements were taken from June 22 through August 15, 2000 on all species except alder. Sap flux for alder was recorded using a Kucera-type sensor [17] from July 25 through August 15, 2000. Measurements were recorded every 15 s and then combined to produce 30 min averages. Sap flux was scaled from point measurements using circumferential and radial trends and sapwood area determined from stem cores [15]. Daily sap flux was summed from 05:00 to 05:00 in order to account for nighttime recharge [55]. Stand E_C was determined by multiplying individual tree sap flux by the ratio of sapwood area to unit ground area [15].

Temperature and relative humidity were recorded in each stand. Photosynthetically active radiation (PAR) was recorded above the cedar stand. Additional measurements were recorded at the WLEF tower and at micrometeorological stations in mixed hardwood, red pine, and alder stands surrounding the WLEF tower. Measurements at these additional sites included wind speed, temperature, precipitation, soil moisture, and relative humidity.

2.3. The TREES model

2.3.1. Model overview

The terrestrial regional ecosystem exchange simulator (TREES) is an integrated hydrology and ecosystem model (Fig. 1; Table 1). Portions of the model are taken from RHESys [44,46], including (1) daily soil water accounting, (2) inter-annual carbon balance, and (3) daily nutrient dynamics. Added to these is a new mechanistic diurnal canopy model for photosynthesis and transpiration [2]. The added mechanistic detail allows TREES to be parsimonious with the detailed diurnal meteorological, sap flux, eddy covariance, and soil moisture data that is being collected around the WLEF eddy flux tower in northern Wisconsin and at other intensive observational sites. In addition, TREES supports dividing the canopy into layers when more detailed canopy structure, micrometeorology and chemistry data are available. For this study we did not make detailed vertical canopy measurements to justify all these mechanisms, and so TREES was operated in a “big leaf” mode, which uses only a single canopy layer and a Jarvis [34] type canopy conductance model.

2.3.2. Canopy transpiration model parameters

E_C is calculated using P–M (Eq. (1)). Canopy absorbed radiation was calculated using the Beer–Lambert

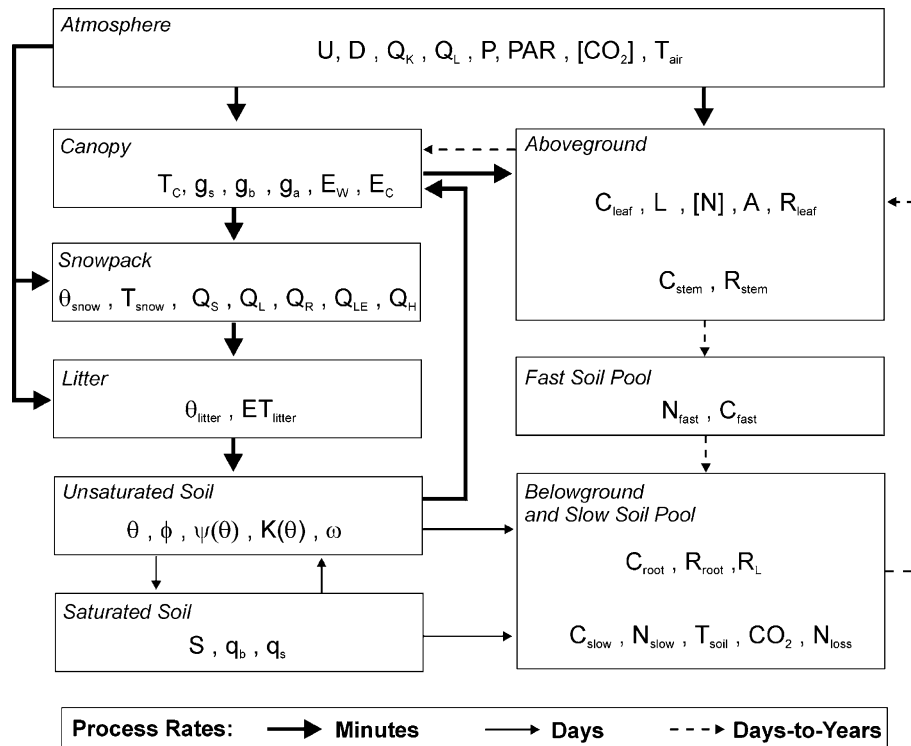


Fig. 1. This is a flow diagram for the TREES. It identifies three primary temporal scales of operation. Diurnal processes are those that operate sub-daily. They include canopy conductance, transpiration and photosynthesis, as well as evaporation from the ground (snowpack or littoral zone). Daily processes are those that deal with water storage and flux in the soil, mineralization of nitrogen, soil CO₂ flux, and nitrate leaching. Carbon allocation processes are maintained at daily-to-annual time intervals depending on the requirements and type of ecosystem. Explanations for the individual terms are given in Table 1.

law to attenuate incoming short-wave radiation through the canopy

$$Q_a = Q_s(1 - \alpha_c)(1 - e^{-kL}), \quad (6)$$

where Q_s is the incoming short-wave radiation (W m^{-2}), α_c is the canopy albedo, and k is the light extinction coefficient. The light extinction coefficient is calculated diurnally (at the frequency of meteorological inputs) based on a general ellipsoidal leaf angle distribution (LAD) [12]:

$$k(\psi) = \frac{\sqrt{x^2 + \tan^2 \psi}}{x + 1.77(x + 1.182)^{-0.0733}} \quad (7)$$

where ψ is the zenith angle of the sun and x is the ratio of average projected areas of canopy elements on horizontal and vertical surfaces. We applied Eq. (7) with $x = 1$, which meant that $k(\psi)$ was more specifically a spherical LAD. Spherical LAD is often assumed when detailed measurements of LAD are not available [12].

TREES calculates canopy aerodynamic resistance using a logarithmic wind speed profile [51]:

$$r_a = \frac{\ln[(z - d/z_0)]}{\kappa^2 u}, \quad (8)$$

where z_0 is the surface roughness ($= 0.1h$), h is the mean tree height (m), d is the zero plane displacement

($= 0.65h$), κ is the von Karman constant ($= 0.4$), and u is wind speed at height z (m). Wind speed data was not available directly above each canopy, but was available at 2 m above the ground in each of the ecosystem types (pine, aspen, northern hardwood, and wetland). We used a profile of canopy wind speed [12] to extrapolate wind speed measurements from below the canopy to the top of the canopy:

$$u_b = u \cdot e^{a(z/h-1)}, \quad (9)$$

where u_b is wind speed at the measurement height below the canopy and a is a wind attenuation coefficient that varies according to canopy architecture [29]. R_a was then calculated from u .

Canopy level stomatal resistance is determined as:

$$r_c = \frac{1}{g_s L}, \quad (10)$$

where g_s is the leaf-level stomatal conductance (m s^{-1}) determined from a multiple constraint function (see also Eq. (3)):

$$g_s = g_{s\max} \cdot f_1(D) \cdot f_2(\Psi_L) \cdot f_3(Q) \quad (11)$$

where with $f_1(D)$ calculated as

$$f_1(D) = 1 - \delta \cdot D, \quad (12)$$

Table 1
Descriptions and relevant references for the symbols in Fig. 1

Module	Symbol	Description	Source	
<i>Atmosphere</i>	U	Wind speed (m s^{-1})	Measured; [12]	
	D	Vapor pressure deficit (kPa)	Measured	
	Q_K	Short-wave radiation ($\text{KJ m}^{-2} \text{s}^{-1}$)	PAR/0.47	
	Q_L	Long-wave radiation ($\text{KJ m}^{-2} \text{s}^{-1}$)	[12]	
	P	Precipitation	Measured	
	PAR	Photosynthetically active radiation ($\text{KJ m}^{-2} \text{s}^{-1}$)	Measured	
	[CO₂]	CO₂ concentration (PPM)	Measured	
<i>Canopy</i>	T_{air}	Air temperature ($^{\circ}\text{C}$)	Measured	
	T_C	Canopy temperature ($^{\circ}\text{C}$)	Measured/computed	
	g_s	Stomatal conductance (m s^{-1})	[34]	
	g_b	Boundary layer conductance (m s^{-1})	[13]	
	g_a	Aerodynamic conductance (m s^{-1})	[49]	
	E_w	Canopy evaporation (m)	[34]	
	E_C	Canopy transpiration (m)	[34]	
<i>Snowpack</i>	θ_{snow}	Snow water equivalent (m)		
	T_{snow}	Snow temperature (C)		
	Q_S	Snowmelt from shortwave radiation (m)		
	Q_L	Snowmelt from longwave radiation (m)		
	Q_R	Snowmelt from rain-on-snow (m)		
	Q_{LE}	Snowmelt from latent heat flux (m)		
	Q_H	Snowmelt from sensible heat flux (m)		
<i>Litter</i>	θ_{litter}	Litter water content (m)		
	ET_{litter}	Litter evaporation (m)		
<i>Unsaturated soil</i>	θ	Soil water content (–)	Measured	
	φ	Porosity (–)	[14]	
	ψ(θ)	Soil water potential (kPa)	[14]	
	K(θ)	Hydraulic conductivity (m s^{-1})	[14]	
<i>Saturated soil</i>	ω	Capillary rise (m)	[28]	
	S	Soil saturation deficit (m)	[65]	
	q_b	Saturated throughflow (m)	[65]	
<i>Aboveground</i>	q_s	Runoff from saturated areas (m)	[65]	
	C_{leaf}	Leaf carbon (kg C ha^{-1})	[44]	
	L	Leaf area index	[11]	
	[N]	Leaf N concentration (kg N kg C^{-1})	[42]	
	A	Assimilation rate (g C s^{-1})	[20,21]	
	C_{stem}	Stem carbon (kg C ha^{-1})	[44]	
	R_{leaf}	Leaf growth and maintenance respiration (kg C ha^{-1})	[54]	
	R_{stem}	Stem growth and maintenance respiration (kg C ha^{-1})	[54]	
	<i>Fast soil pool</i>	N_{fast}	Fast soil nitrogen pool (kg N ha^{-1})	[44]
		C_{fast}	Fast soil carbon pool (kg C ha^{-1})	[44]
CO₂		Fast soil respiration (kg C ha^{-1})	[44]	
<i>Belowground and Slow soil pool</i>	C_{root}	Root carbon (kg C ha^{-1})	[44]	
	R_{root}	Root growth and maintenance respiration (kg C ha^{-1})	[58]	
	R_L	Rooting length (m)	[44]	
	C_{slow}	Slow soil carbon pool (kg C ha^{-1})	[44]	
	N_{slow}	Slow soil nitrogen pool (kg N ha^{-1})	[44]	
	T_{soil}	Soil temperature ($^{\circ}\text{C}$)	[44]	
	CO₂	Slow soil respiration (kg C ha^{-1})	[44]	
	N_{loss}	Nitrogen loss (kg N ha^{-1})	[44]	

Components related to the present study are in bold. The line separating module, Saturated soil, from module, Aboveground, is the division between hydrologic and ecosystem components of TREES.

where δ [$(\text{kPa})^{-1}$] is sensitivity of stomatal conductance to D . From the earlier discussion it is implied that Eq. (12) is only a surrogate for stomatal response to the rate of water loss from the canopy, which is a function of D . $f_2(\Psi_L)$ is a function of soil water availability. Predawn leaf water potential modifies maximum stomatal conductance as:

$$f_2(\Psi_L) = \left[1 - \frac{\Psi_L - \Psi_M}{\Psi_{SC} - \Psi_M} \right], \quad (13)$$

where Ψ_M is leaf water potential at stomatal closure (MPa), and Ψ_{SC} is minimum leaf water potential (MPa) under well-watered conditions. Predawn leaf water

potential is assumed to be equal to soil water potential calculated as:

$$\Psi_L = \Psi_c \left(\frac{\theta}{\phi} \right)^{-b}, \quad (14)$$

where Ψ_c is the air entry water potential (kPa), θ is the predawn soil water content ($\text{m}^3 \text{m}^{-3}$), b is the Brooks and Corey [10] soil pore space connectivity parameter, and ϕ is the soil porosity ($\text{m}^3 \text{m}^{-3}$) [14]. The radiation reduction modifier is calculated as:

$$f_3(Q) = \min \left[\frac{Q_{rl}}{Q_{min}}, 1 \right], \quad (15)$$

where Q_{rl} is absorbed radiation per leaf area ($\text{kJ m}^{-2} \text{L}^{-1}$) and Q_{min} is the minimum threshold radiation ($\text{kJ m}^{-2} \text{L}^{-1}$) for g_s .

2.4. Model parameterization

To analyze the sensitivity of the parameters of our canopy model we used a parameter estimation framework [59] that is based on a number of approaches that have been proposed for hydrologic models [9,31,39,41,66,67,71]. The solutions proposed to account for this uncertainty often accept a set of parameter combinations selected from among many simulations using some form of Monte Carlo sampling. A set of retained parameter combinations allows for ambiguity (or non-specificity) in the selection of model parameters. This non-specificity arises because parameters are often surrogates for something that has not been measured or is poorly known [7,8]. This can result in similar flux estimates using different combinations of poorly conditioned parameter values.

We combined Monte Carlo sampling and measures of uncertainty derived from information processing [62]. One information-theoretic expression of non-specificity is the Hartley function [32]:

$$H(A) = \log_2 |A|, \quad (16)$$

which relates a finite set A to its cardinality $|A|$. If A represents a set of selected combinations of simulation model plus parameter set (henceforth called a “model”), then a higher $|A|$ in proportion to the size of the population of models implies a greater non-specificity in parameter estimation. For example, if 1000 parameter combinations are generated and 900 are determined to give acceptable model results, then this solution set has greater non-specificity than if only 10 model-parameter combinations are retained. Without further conditioning of the parameters we are forced to accept a wide variation in parameter values, which are unreliable for extending model simulations in space and time.

When the acceptable set of models is considered a fuzzy set [76], F , within the domain, X , of all feasible models, uncertainty related to the cardinality of F can

be expressed as a fuzzy logic measure of the non-specificity of F [33,40]:

$$U(F) = \int_0^{h(F)} \log_2 |{}^\alpha F| d\alpha + (1 - h(F)) \log_2 |X|, \quad (17)$$

where $U(F)$ is the U -uncertainty associated with F , $|{}^\alpha F|$ is the cardinality of an α -cut of F (i.e. the number of members that remain in the set if all members with a membership grade less than α are removed from F), $h(F)$ is the height of F (or maximum value of membership grade in F), and $|X|$ is the cardinality of the universal set (i.e. the model population). A numerical solution to Eq. (17) is given by

$$U(r) = \sum_{i=2}^n (r_i - r_{i+1}) \log_2 i + (1 - r_1) \log_2 n, \quad (18)$$

where r is the ordered possibility distribution [77] derived from the fuzzy set F and r_{n+1} is assumed to be 0. Fig. 2 shows a series of hypothetical relationships between $f(x_i)$ and $|{}^\alpha F|$, as well as the physical meaning of the α -cut. At an α -cut of 0.6 the three relationships shown yield very different cardinalities. Relations that are skewed towards the low end, and thus have only a few high $f(x_i)$ models, are better than relations having too many high $f(x_i)$ values. The ideal is to have a single model with $f(x_i) = 1.0$ and all other models with $f(x_i) = 0.0$. This gives a cardinality of 1.0 for the fuzzy set and a cardinality of 1 for the restricted (or crisp) set. The more usual case is one in which the cardinality of the fuzzy set is greater than 1.0.

The key is to objectively define the α -cut needed to form the restricted set from the fuzzy set. Initially, this α -cut should be selected with caution. On the one hand, it may be possible that useful information in the fuzzy set may be lost if an arbitrarily high α -cut is selected. On

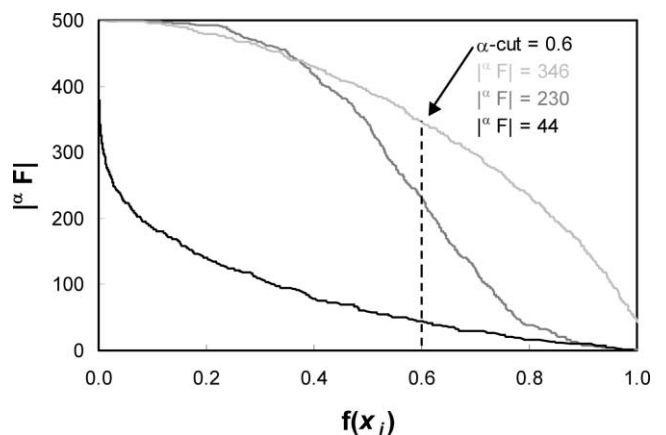


Fig. 2. These hypothetical distribution functions illustrate how cardinality of a candidate set of models varies by value obtained from a measure of goodness-of-fit. At a given level (or -cut) a low cardinality indicates a high level of specificity in the set of candidate models. A high cardinality indicates a high level of non-specificity.

the other hand, an arbitrarily low α -cut may include too many models that are of poor quality. An arbitrarily high α -cut may also admit a false sense of specificity in the model system. An objective way to extract the full information content of a fuzzy set is to apply the principle of uncertainty invariance [40], which transforms a fuzzy set into a restricted set that approximates the respective fuzzy set by virtue of having the same U -uncertainty. The principle of uncertainty variance objectively determines where to apply the α -cut by minimizing $|U(r) - \log_2 k|$ such that the k th element of the ordered possibility distribution is location of the cut. This approach can be demonstrated by applying it to a simple fuzzy set. Consider the ordered fuzzy set $F = \{0.9, 0.8, 0.8, 0.7, 0.6, 0.4, 0.1, 0.1\}$. $|^z F|$ is the sum of fuzzy memberships in the set ($=4.4$) and $U(r) = 2.2$. The size of the restricted set is determined by equating the U -uncertainty of the fuzzy set (Eq. (18)) to the Hartley function (Eq. (16)) for the desired crisp set. The value of k (5 in this example) is the required cardinality of the retained model set, which means that the top five models in F are retained and the α -cut is placed at 0.6. Note that the models are no longer ranked within the restricted set. This is based on the assumption that all the information obtainable from a particular objective function has been extracted in constructing the restricted set. No further ranking is allowed within this set based on the same objective function. An advantage of this approach is that the threshold position is repeatable from the data and not subject to interpretation or modification as the goals of a modeling exercise change. A disadvantage of the approach is that it is naïve, in that it does not consider intuition about the physical system, which is an essential part of parameter estimation. However, once we have objectively established the extent of parameter values from the information content of the fuzzy set, then we can proceed to make successively higher α -cuts given additional knowledge.

TREES parameter estimation was conducted for each species as described in Ahl et al. [2]. The range for each parameter was adjusted after initial simulations to maximize the number of parameter values selected over the range for each respective parameter. This involved executing the model and comparing simulation output to sap flux E_C . In this way, we were able to select the most sensitive parameters and their value ranges for each species. The parameters and their ranges were Q_{\min} (30–790) [57], $g_{S\max}$ (0.4–5) [38], δ (0.07–0.74) [34], a (0.5–4.0) [47], and for alder only, r_a (1–200) [37]. For each species, 15,000 simulations were performed with random parameter values within the ranges defined for each parameter. Simulations were run at 30-min time-steps using 30-min average micrometeorological data collected for each stand type, and E_C was output on a daily timestep. Each simulation set was evaluated using a linear regression analysis of the form:

$$\hat{E}_C = b_0 + b_1 \cdot E_C, \quad (19)$$

where b_0 and b_1 are regression coefficients referred to as the intercept and slope, respectively, \hat{E}_C is the simulation estimate of E_C (mm day⁻¹). Simulation results were evaluated using the regression coefficients and the coefficient of determination calculated as

$$R^2 = \left\{ \frac{\sum_{i=1}^N (E_C - \overline{E_C})(\hat{E}_C - \overline{\hat{E}_C})}{\left[\sum_{i=1}^N (E_C - \overline{E_C})^2 \right]^{0.5} \left[\sum_{i=1}^N (\hat{E}_C - \overline{\hat{E}_C})^2 \right]^{0.5}} \right\}^2. \quad (20)$$

To evaluate all three criteria, b_0 , b_1 and R^2 , simultaneously we combined them into a single index, as follows [2]:

$$f(x_i) = I = 1 - \max \left\{ \left[w_1(b_0 - 0)^2 + w_2(b_1 - 1)^2 + w_3(1 - R^2)^2 \right]^{0.5}, 0 \right\}, \quad (21)$$

where I describes the relative deviation of the regression parameters and R^2 from an ideal model ($I = 1$) and $w_1 + w_2 + w_3 = 1$ are weighting factors. A model was considered to be a good predictor of transpiration when its respective regression with sap flux data had an intercept near 0, a slope near 1, and a high R^2 . For this study, $w_1 = w_2 = w_3$ as we did not want to give preferential weight to any one criteria for the goodness-of-fit. It was assumed that models that yield high I -values were likely to be the best predictors of transpiration.

3. Results and discussion

3.1. Stand-level parameter estimation

Fig. 3 shows the calibrated TREES canopy transpiration for each of the five species simulated for the “optimal” model (i.e., highest I score, Eq. (21)). There is a large variation of E_C among species, but given that this represents a continuous simulation over a two-month period the model performs well for all stands. Transpiration showed a marked increase in the second half of the summer for red pine [15], which lowered the performance of the model for this species. By handling different parameter sets for the first and second halves of the data period, Ahl [2] showed an improved model fit to the measurements (Fig. 3, “Red Pine Split Model”). A number of factors could explain such a time trend in transpiration for the red pine. Referring to Eq. (4), the trend could be explained by a change in K_L , which may be caused by increased biochemical activity in new foliage, changes in hydraulic properties within the trees, or some combination of factors. We have found no environmental factors that explain this result [15]. Without

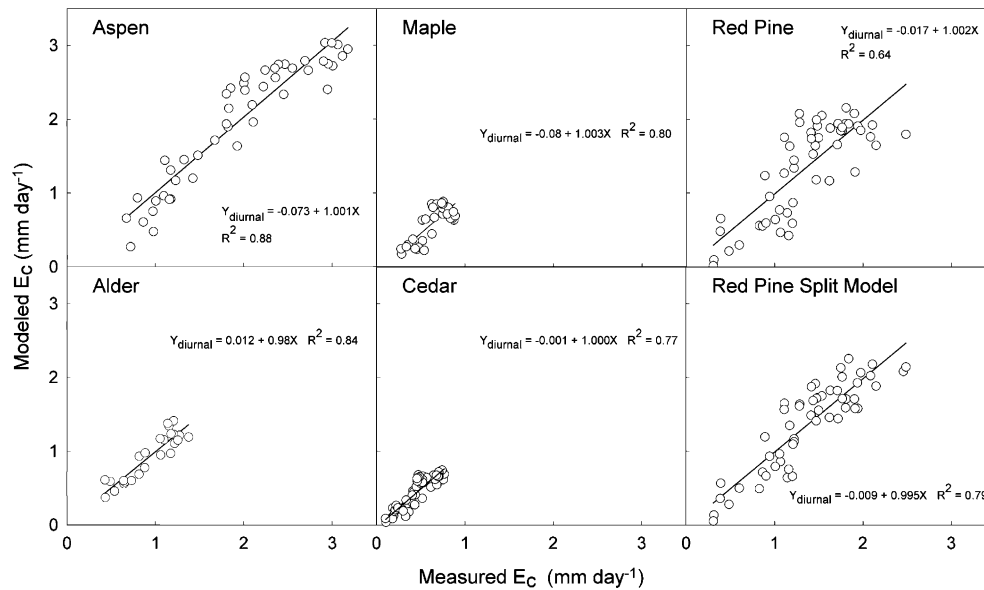


Fig. 3. TREES canopy transpiration for five major northern Wisconsin forest species. The results are from the model with the highest I (see Eq. (21)). The red pine transpiration showed a seasonal trend [15] and so a split model is provided in which parameter values are allowed to differ between the first half of the summer and the second half.

further data we can only speculate on a mechanism to explain the trend. For this reason we do not present parameter analysis for the split model for red pine.

Fig. 4 shows cumulative possibility distribution functions for each of the five species. The aspen shows the closest to a normal distribution, while the others are closer to an uniform distribution. With the exception of cedar all distributions show a pronounced tail at the high membership values. This tail shows, that, while there are potentially many good models, there are relatively few exceptionally good ones. As such, it is acceptable to explore making higher α -cuts, than those calculated completely objectively by minimizing $|U(r) - \log_2 k|$. Table 2 summarizes the results of applying Eqs. (18)–(21), using three α -cuts determined (1) by minimizing $|U(r) - \log_2 k|$, (2) from the top 1000 models, and (3) from the top 100 models for each species. Red pine and cedar show relatively high $h(F)$ and $|^2F|$ with the objective α -cuts obtained using the principle of uncertainty invariance. This indicates that these stands are influenced by tradeoffs among the parameters, which make it difficult to objectively restrict the solution set. Fig. 5 shows the corresponding combinations of $g_{S_{\max}}$ and δ . The objective selection of α -cut for cedar and sugar maple show a very definite clustering with respect to these parameters. For maple, cedar, and red pine, a saturating curve describes the relationship between $g_{S_{\max}}$ and δ . A similar, but somewhat more scattered, pattern exists for the aspen $g_{S_{\max}}$ and δ cluster. Alder shows little or no relationship between these parameters.

These differences in responses among species may be partly explained in terms of whole canopy coupling

with the atmosphere. Different canopies can be classified in terms of degree of coupling. Jarvis and McNaughton [36] defined this with a coupling coefficient, Ω , which varied from one (low boundary-layer conductance, g_b , in proportion to g_s) to zero (high g_b , in proportion to g_s). Red pine and cedar would be expected to have low Ω values, as red pine is a plantation with well-spaced crowns and the cedar has well-spaced, individual crowns emerging above an alder under-story. The maple stand also shows a tight clustering with respect to $g_{S_{\max}}$ and δ , which would support it having low Ω . This may be explained in part by the fact that it was thinned less than ten years prior to this study. Aspen and alder appear to have higher Ω as evidenced by their more poorly formed clusters. The alder are relatively short trees with broad leaves, are sitting in water, and therefore are influenced by free evaporation from the forest floor and low wind speed in the canopy. Aspen has a relatively open canopy, but it also has high $g_{S_{\max}}$, which means that g_b may be small in proportion to g_s .

Within each stand we retained the restricted sets of 100 models, which were then sorted by Q_{\min} . We selected ten models from each of low, medium and high Q_{\min} (Fig. 6). Red pine and cedar show well-defined light saturation, as indicated by the clustering of high Q_{\min} values on the saturating part of their respective curves. Maple shows a moderate amount of clustering by Q_{\min} but aspen and alder show only a slight organization by light. Species with well-defined light saturation curves clearly exhibit high parameter non-specificity. A reduction in g_s can be achieved with an increase in either or Q_{\min} . Without further conditioning to reduce these

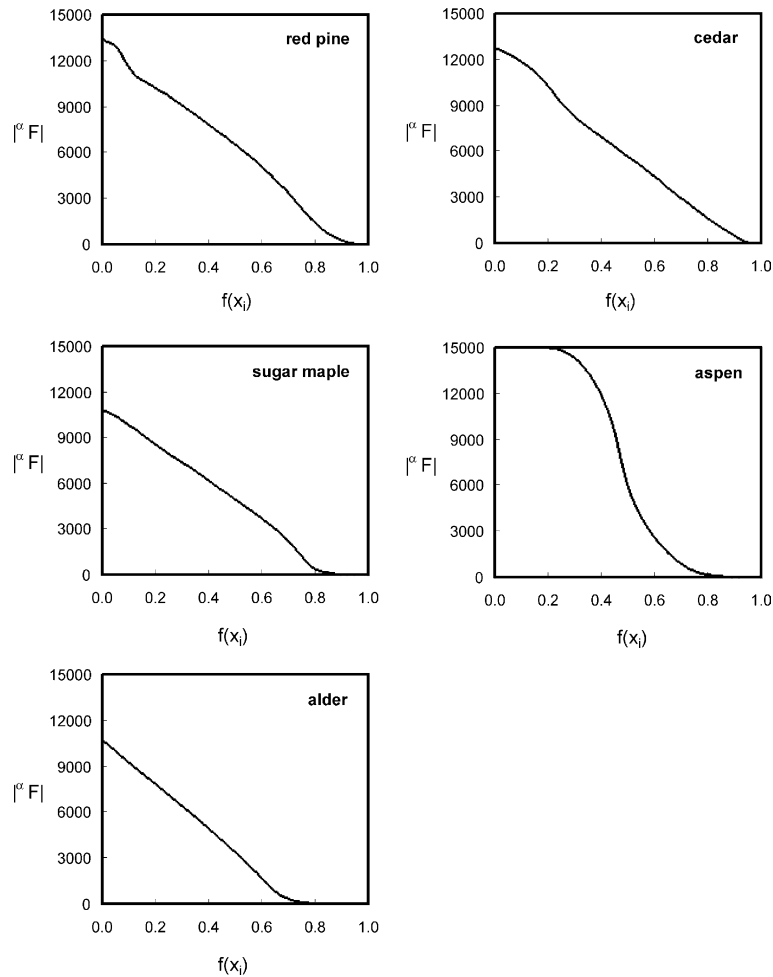


Fig. 4. Shown are possibility distributions (Eq. (18)) for the 15,000 simulations for each of the five tree species.

Table 2

Summary of U -uncertainty parameters for each tree species type, determined from among 15,000 simulations per stand

Species	$h(F)$	$U(F)$	$ ^z F $	α -cut	α -cut $ ^z F = 1000$	α -cut $ ^z F = 100$
Alder	0.909	10.651	1608	0.603	0.638	0.752
Aspen	0.918	11.639	3190	0.575	0.689	0.820
Cedar	0.976	11.871	3745	0.641	0.851	0.939
Red pine	0.979	11.841	3759	0.683	0.826	0.928
Sugar maple	0.946	11.310	2539	0.680	0.759	0.855

parameter tradeoffs it is not possible to reliably parameterize the canopy physiological controls on water fluxes at even the forest stand level.

3.2. Physiologic interpretation of parameter tradeoffs

The results thus far suggest that the parameter tradeoffs ($g_{S_{\max}}$ versus δ) seen in the simulations indicate that the Jarvis-type model captures stomatal regulation of water potential. However, other factors may contribute to this apparent physically consistent behavior of the parameters. There may be just enough degree of freedom in our choice of parameters to allow for an

acceptable fit to the sap flux E_C . In other words, we cannot yet state that TREES captures the processes any more than a multivariate statistical approach would. To assign a direct physical interpretation to the apparent relationships between $g_{S_{\max}}$ and δ (Fig. 5), we translated these parameters into $G_{S_{\text{ref}}}$ and $dG_S/d \ln D$, respectively, as expressed by the tree hydraulic equations (Eqs. (4) and (5)). The $g_{S_{\max}}$ parameter is implicitly assumed to represent a theoretical optimal value that could be obtained under ideal conditions. From Eq. (12) it follows that $g_s = g_{S_{\max}}$ if and only if $D = 0$ kPa. It is not possible to measure g_s at $D = 0$ kPa, and so we transformed $g_{S_{\max}}$ into $G_{S_{\text{ref}}}$ [17] as follows:

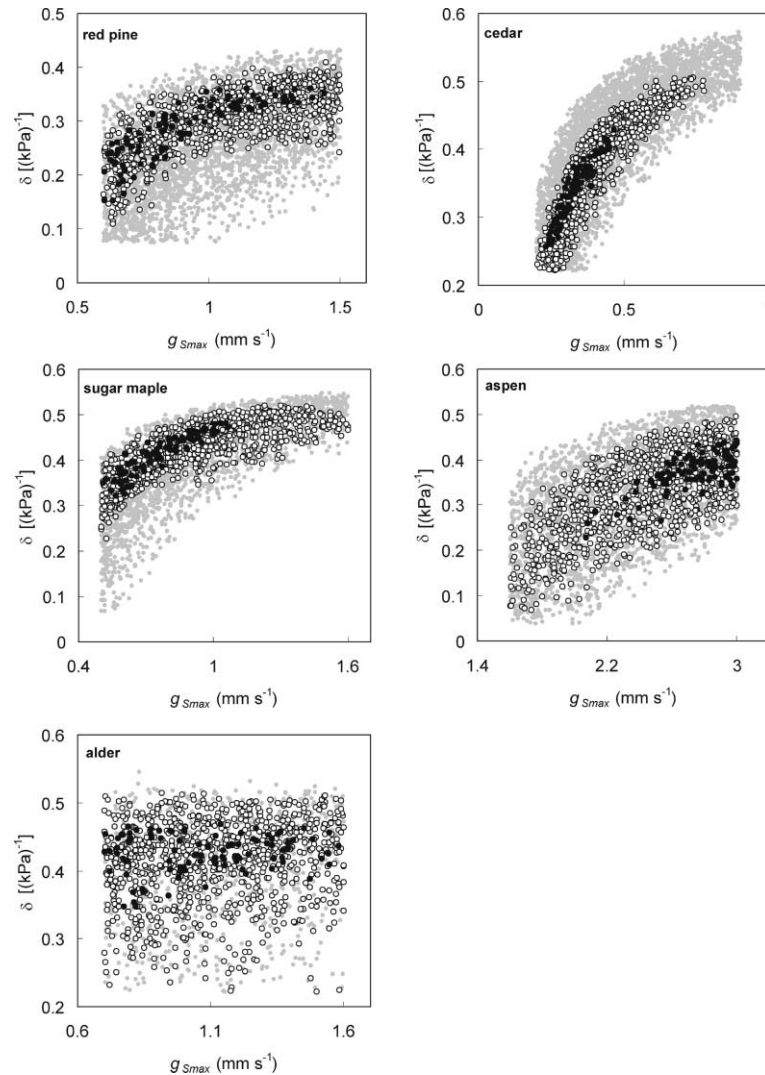


Fig. 5. Shown is stomatal sensitivity to vapor pressure deficit versus maximum stomatal conductance for different tree species in northern Wisconsin. Light gray circles represent models retained using the principal of uncertainty invariance. The open circles are the best 1000 models, and the closed circles are the best 100 models. Axes are shown with different ranges to highlight the distribution of parameter values for each species.

$$G_{Sref} = g_{Smax}(1 - \delta) \quad (22)$$

and converted δ to $dG_S/d \ln D$ as follows:

$$dG_S/d \ln D = g_{Smax} \cdot d\delta/d \ln D, \quad (23)$$

which was calculated by determining the slope between $D = 0.6$ kPa and $D = 1.4$ kPa. We chose the lower D on the grounds that this represents a threshold above which errors in many of the measurements (including D and sap flux) drop to 15% or less [16].

Fig. 7 shows the results for the best 100 models for the respective stands. All stands fall on or near the theoretical 0.6 line predicted to occur if stomata are regulating water potential to just prevent runaway cavitation [53]. Aspen shows a bias towards falling below this line, which would suggest that not all models within its cluster follow the theory. The red pine cluster also falls a moderate distance below the theoretical line. The

cedar and sugar maple clusters have steeper slopes, and so they tend to have higher than expected $dG_S/d \ln D$ with increasing G_{Sref} . One explanation for this, is, that parameter tradeoffs with Q_{min} are producing conditions that are not physically reasonable. For example, high Q_{min} tends to occur on the saturating or high end of the versus g_{Smax} curves. Fig. 8 shows more restricted clusters selected based on ten Q_{min} values that envelope the optimal model for each species, determined by sorting the top 100 models by Q_{min} . All optimal models, with the exception of red pine, fall on or near the 0.6 line, and the clusters converge to this line. Furthermore, ensembles of 30 models grouped by Q_{min} also strongly fit the 0.6 line, as shown in the inset figure in Fig. 8. The convergence of model parameters to small clusters sitting on or near the theoretical line supports the claim that the TREES model is resolving inter-specific differences in

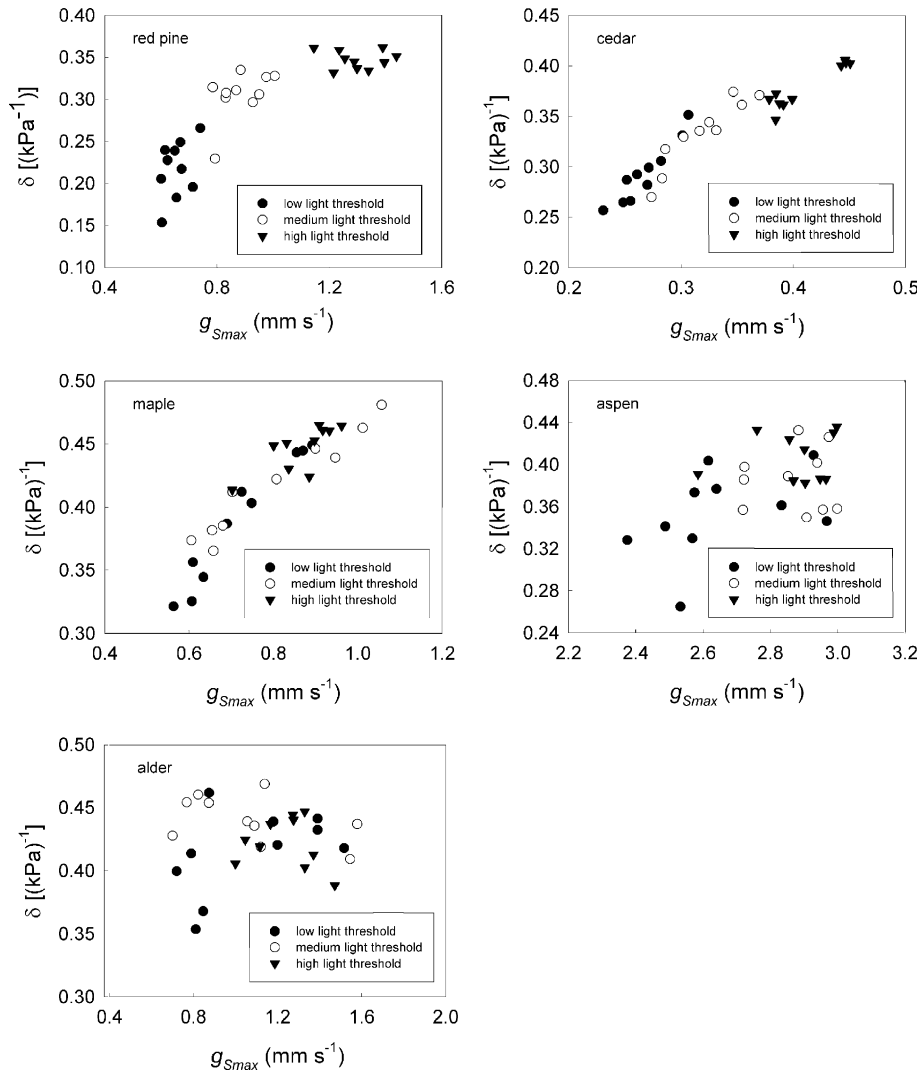


Fig. 6. This figure shows subsets of the clusters shown in Fig. 4, obtained by sorting the top 100 models in each species by the light threshold parameter. The plots show the tradeoffs between δ and g_{Smax} for the models with the lowest ten, middle ten, and highest ten light threshold values. Axes are shown with different ranges among species to highlight parameter clusters for each species.

hydraulic control on canopy transpiration rather than simply being over parameterized. This claim is not fully supported in the case of red pine. One possibility is that red pine has a lower set point for leaf water potential, and so its stomata do not work as hard to regulate water potentials under the relatively moderate D that typically occurs in northern Wisconsin. This could also be attributed to the time trend observed in the red pine transpiration data [15], since a seasonal trend in the water potential set point is one of a number of physiological changes that can theoretically occur (see Eq. (4)). Oren et al. [53] found that species falling below the theoretical $m \approx 0.6 G_{Sref}$ line do not regulate their water potentials; they include desert species, which have low minimum water potentials. This adaptive behavior does not appear to explain the red pine response, as the slope of the red pine cluster in Fig. 7 is nearly parallel to the

theoretical line. Another possibility is that the red pine parameter values are compromised by the unexplained seasonal trend in transpiration [15]. Further data on seasonal trends is needed to resolve this issue.

We currently do not have a robust means of evaluating Q_{min} . In the present analysis, Q_{min} appears to be useful for narrowing the range of g_{Smax} and δ parameters to those that most closely follow the regulation of water potential. For the species with obvious saturating curves (red pine, cedar, Fig. 6), Q_{min} allows for the rejection of the saturating portion of the curve. In all species, the final range of g_{Smax} and parameters are from low-to-moderate values from among the top 100 models in each species. Since water fluxes are low when Q_{min} is expected to have the greatest affect on stomatal conductance, an increase in this parameter would be costly in terms of reduced carbon gain with only a marginal reduction in

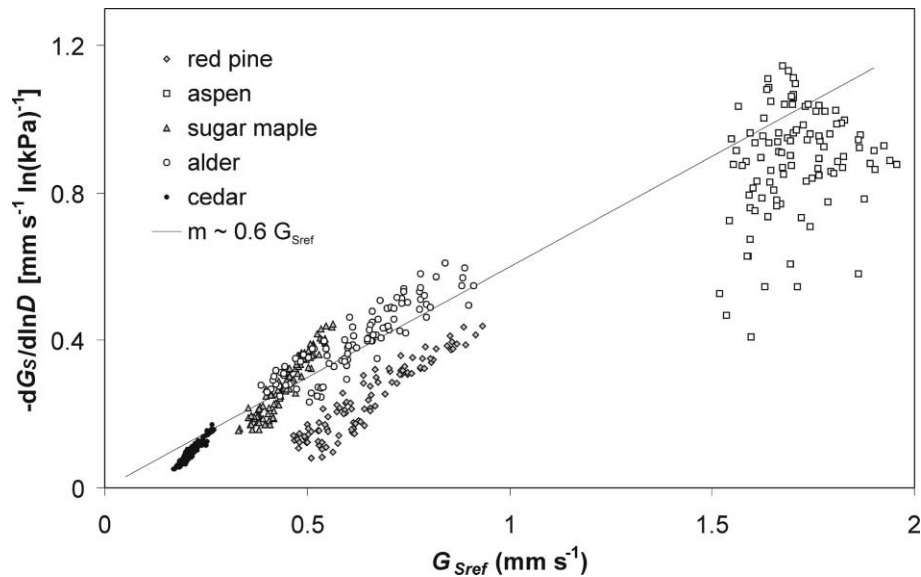


Fig. 7. The plots shown in this figure were derived by converting the model input of g_{Smax} to G_{Sref} at $D = 1$ kPa using a reduction of δ , and then determining the rate of decline of G_S with $\ln D$ by taking G_S at $D = 2$ (i.e. using a reduction of δ). Each point represents a model (TREES plus parameter set) and the 100 models with the highest calibration fit to the sap flux are plotted. The 0.6 line was determined by Oren et al. [53] to hold for most species that have stomatal regulation of leaf water potential.

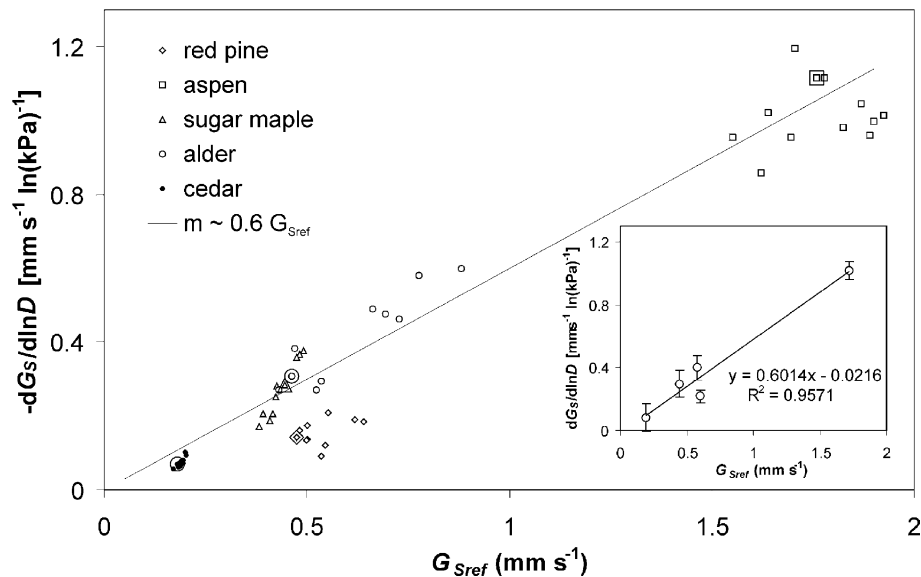


Fig. 8. The points shown in this figure are a subset of the points in Fig. 7. Subsets of models were selected by clustering them by light threshold. The larger, open dots represent the model with the highest calibrated fit to the sap flux data. The inset plot shows ensemble (30 models grouped by light threshold) averages with the bars showing average deviation from the average. The 0.6 line was determined by Oren et al. [53] to hold for most species that have stomatal regulation of leaf water potential.

water loss. Consider, for instance, the red pine, which shows a pronounced light saturation (see Fig. 6). The optimal model and the models that cluster around it are obtained from the upper end of the lower cluster of Q_{min} . This can be explained by looking at the relative values for the optimal parameters in comparison to the safe and efficient parameter sets (Table 3). Both g_{Smax} and Q_{min} are reduced for the optimal simulation, indicating

that the light saturation is forcing TREES to contradict hydraulic theory. This indicates that models falling within the saturating portion of the $g_{Smax}-\delta$ curve (Fig. 6), and hence falling off the 0.6-line, can be considered artifacts of over-parameterization. The alder is much more sensitive to light within the operating conditions allowed by the hydraulic theory, as evidenced by the fact that its cluster (see Fig. 8) spans a relatively wide range

Table 3

Parameter adjustments made for the physiological tradeoffs between safety and efficiency of gas exchange, as well optimal models

Species	Model	Q_{\min} (kJ m ⁻² 30 min ⁻¹)	$g_{S_{\max}}$ (mm s ⁻¹)	δ (kPa) ⁻¹	a^a (-)
Alder	Safety	241.0	0.70	0.430	119.6
	Efficiency	165.6	1.60	0.444	15.2
	Optimal	39.0	0.79	0.415	50.7
Aspen	Safety	33.2	2.10	0.230	1.0
	Efficiency	73.9	3.00	0.437	1.4
	Optimal	47.5	2.70	0.400	1.9
Cedar	Safety	46.5	0.23	0.259	0.9
	Efficiency	143.1	0.47	0.430	2.0
	Optimal	92.7	0.30	0.341	2.3
Red pine	Safety	58.7	0.60	0.156	4.4
	Efficiency	193.8	1.40	0.348	3.6
	Optimal	110.0	0.83	0.304	1.3
Sugar maple	Safety	44.1	0.50	0.348	1.2
	Efficiency	69.0	1.10	0.474	2.3
	Optimal	32.5	0.70	0.385	2.4

^a For alder the a parameter was replaced with a r_a , (s m⁻¹) as the wind speed data was corrupt for the understory wetland.

of $G_{S_{\text{ref}}}$ and its optimal Q_{\min} is well below the values for the respective safe and efficient models. This is consistent with the analysis of diurnal sap flux in alder, which shows a more significant response to Q than to D [15].

There is a clear tradeoff between $g_{S_{\max}}$ and δ parameters, which means that, within the same set of data, it is possible to have different strategies to reduce transpiration. Daily transpiration can be reduced either by reducing $g_{S_{\max}}$ or increasing δ . To interpret these results in terms of their physiological significance we refer to Eqs. (4) and (5). To prevent runaway cavitation a plant either needs to have a low set point for its leaf water potential, which requires a high structural integrity of its cell walls (or low vulnerability to cavitation), or it must safeguard against high leaf water potentials by closing stomata. It has been shown that species regulating their water potentials do so by following a universal relationship (Eq. (5)) between $G_{S_{\text{ref}}}$ (and also $g_{S_{\max}}$) and sensitivity to D [53] (also δ). Where a species lies along the universal line ($m \approx 0.6 G_{S_{\text{ref}}}$) may be determined from knowledge of its vulnerability to cavitation [15]. On one hand, the “efficiency” associated with a high $g_{S_{\max}}$ comes at a cost, as high K_L per unit L is needed to meet the high demand for water, and this makes the plant vulnerable to hydraulic failure [18]. All other components of the hydraulic equation (Eq. (4)) being equal, aspen appears to be at greater risk of hydraulic failure than the other species in this study, as it operates with high stomatal conductance under optimal conditions. On the other hand, the “safety” associated with a low $G_{S_{\text{ref}}}$ means the plant can have a lower K_L per unit L . While this reduces its vulnerability to hydraulic failure when water is limiting or atmospheric demand for water is high [18] it also compromises the photosynthetic capacity when water supply exceeds demand. Cedar is the most extreme example of

this latter strategy. The other species lie between the safety and efficiency extremes observed by cedar and aspen, respectively.

The physiological significance of these observations can also be considered in terms of carbon gain and plant growth. Species operating with high $g_{S_{\max}}$ (e.g., aspen) are better able to take advantage of optimal environmental conditions to maximize CO₂ gain than species operating with low $g_{S_{\max}}$ (e.g., cedar). In our study sites, aspen is a fast-growing species with a high rate of carbon uptake and a relatively short life-span. Cedar is a relatively slow-growing species, but is relatively long-lived. Their contrasting physiologies have important implications for land surface process modeling of water and carbon storage and flux, from short to long timescales, across a heterogeneous landscape. The safety versus efficiency tradeoffs embodied by Eq. (5) provides a direct physical connection between model parameterization and the physiological functioning of cohorts of vegetation types. As such, this model could be considered complementary to the traditional land surface parameterization schemes based on biome classification coupled with remote sensing [60,64,78]. Parameterization of the variability in canopy physiology among species could then amount to mapping the land surface into positions along the continuum between safe and efficient strategies. This could greatly simplify the task of parameterizing for species-specific functioning at large scales.

Among species differences in physiological response to D , in particular, would be expected to produce a wide range of spatial variability in transpiration in a heterogeneous forest landscape, such as exists around the WLEF tower. The spatial variations are expected to be smallest at low D , when transpiration rates are small, and possibly of minor significance for catchment scale

hydrologic modeling. The greatest spatial variations in transpiration would be at intermediate levels of D , during which time inter-species differences in strategies for regulating leaf water potential would have the most pronounced effect. As D is increased from low values, the aspen and red pine would have proportionally the highest increases in E_C . Alder would provide a moderate increase in flux, but cedar and sugar maple would not increase as much due to their low stomatal conductance. Aspen, with the highest E_C , would also show the greatest decline at the highest levels of D . This follows from the argument that stomatal closure would more than offset the increased evaporative demand, as first suggested by Jarvis [35] and shown empirically by Pataki et al. [54]. Given its high stomatal conductance and sensitivity to D , the aspen trees we measured operate with low safety margins for hydraulic failure [18]. The implications of these dynamics for land surface process models that use aggregate biomes rather than species-specific details are significant. Biome type models may capture the spatial variability of water fluxes when evaporative demand is low and also when the vegetation is stressed. However, it is in the transition between these states where differential responses to vapor pressure deficits are most pronounced among species, and much of the growing season for vegetation in temperate climates is characterized by moderate vapor pressure deficits.

4. Conclusions

The Jarvis-based canopy conductance model in TREES is able to accurately simulate daily transpiration for a range of tree species. More importantly, the tradeoffs found between maximum stomatal conductance and stomatal sensitivity to vapor pressure deficit are consistent with theory on the regulation of leaf water potential. Differences in canopy coupling among species did not preclude finding hydraulically consistent parameter combinations, owing to the fact that model behavior over a long period is less sensitive to coupling than would be expected for shorter periods of time, such as for diurnal simulations. Among-species differences in strategies for regulating leaf water potential would result in large inter-species differences in dynamic response to changing environmental conditions. The implication is that land surface process models that ignore these differences may under predict the spatial and temporal variability of transpiration. While these differences may not be large when considered at regional to global scales, they may dominate the dynamic response at scales of flux towers and catchments. Furthermore, the non-linearity of the dynamic responses would not cancel out over time, and so large biases may be possible. Our results indicate that species-specific knowledge can be assimilated to improved model logic. The improved

model could be applied beyond the stand if the universal scaling of stomatal regulation of leaf water potential can be developed into a proxy for the species-specific details and combined with existing land surface parameterization schemes.

Acknowledgements

Funding for this research was provided from the NASA Land Surface Hydrology Program (NAG5-8554). Additional funding from the Wisconsin Alumni Research Foundation (WARF) and McIntire-Stennis are also acknowledged. Computing facilities of the UW-Madison Integrated Remote Sensing Resources Center, a NASA Center of Excellence in Remote Sensing (NAG5-6535), were used in this research. We thank the many undergraduate students who assisted with data collection and processing.

References

- [1] Aber JD, Federer CA. A generalized, lumped-parameter model of photosynthesis, evapotranspiration and net primary production in temperate and boreal forest ecosystems. *Oecologia* 1992;92:463–74.
- [2] Ahl DE. A measurement and modelling perspective on requirements for future remote sensing vegetation indices and classifications. Unpublished Ph.D. dissertation, Environmental Monitoring, Institute for Environmental Studies, University of Wisconsin-Madison, 2002. 181 pp.
- [3] Arnold JG, Srinivasan R, Muttia RS, Williams JR. Large area hydrologic modeling and assessment part I: model development. *J Am Water Resour Assoc* 1998;34(1):73–89.
- [4] Bakwin PS, Tans PP, Hurst DF, Zhao CL. Measurements of carbon dioxide on very tall towers: results of the NOAA/CMDL program. *Tellus Ser B—Chem Phys Meteorol* 1998;50:401–15.
- [5] Ball JT, Woodrow IE, Berry JA. A model predicting stomatal conductance and its contribution to the control of photosynthesis under different environmental conditions. In: Biggens J, editor. *Progress in Photosynthesis Research*, vol. IV. Dordrecht, The Netherlands: Martinus Nijhoff Publishers; 1987. p. 221–9.
- [6] Band LE, Patterson P, Nemani R, Running SW. Forest ecosystem processes at the watershed scale: incorporating hillslope hydrology. *Agri Forest Meteorol* 1993;63:93–126.
- [7] Beven KJ. Changing ideas in hydrology: the case of physically-based models. *J Hydrol* 1989;105:157–72.
- [8] Beven KJ, Binley A. The future of distributed models: model calibration and uncertainty prediction. *Hydrol Process* 1992; 6:279–98.
- [9] Binley AM, Beven KJ. Physically-based modeling of catchment hydrology: a likelihood approach to reducing predictive uncertainty. In: Farmer DJ, Rycroft MJ, editors. *Computer modelling in the environmental sciences*, IMA Conference Series. Oxford: Clarendon Press; 1991. p. 75–88.
- [10] Brooks RH, Corey AT. Hydraulic properties of porous media. *Hydrology Paper 3*, Colo. State University, Fort Collins, 1964. p. 27.
- [11] Burrows SN, Gower ST, Clayton MK, Mackay DS, Ahl DE, Norman JM, Diak G. Application of geostatistics to characterize leaf area index (LAI) from flux tower to landscape scales using a cyclic sampling design. *Ecosystems* 2002;5(7):667–79.

- [12] Campbell GS, Norman JM. An introduction to environmental biophysics. New York: Springer; 1998.
- [13] Choudhury BJ, Monteith JL. A four-layer model for the heat budget of homogeneous land surfaces. *Quart J Roy Meteorol Soc* 1988;114:373–98.
- [14] Clapp RB, Hornberger GM. Empirical equations for some soil hydraulic properties. *Water Resour Res* 1978;14:601–4.
- [15] Ewers BE, Mackay DS, Gower ST, Ahl DE, Burrows SN, Samanta S. Tree species effects on stand transpiration in northern Wisconsin. *Water Resour Res* 2002;38(7).
- [16] Ewers BE, Oren R. Analyses of assumptions and errors in the calculation of stomatal conductance from sap flux measurements. *Tree Physiol* 2000;20:579–89.
- [17] Ewers BE, Oren R, Johnsen KH, Landsberg JJ. Estimating maximum mean canopy stomatal conductance for use in models. *Can J Forest Res* 2001;31:198–207.
- [18] Ewers BE, Oren R, Sperry JS. Influence of nutrient versus water supply on hydraulic architecture and water balance in *Pinus taeda*. *Plant Cell Environ* 2000;23:1055–66.
- [19] Famiglietti JS, Wood EF. Multi-scale modeling of spatially variable water and energy balance processes. *Water Resour Res* 1994;30:3061–78.
- [20] Farquhar GD, von Caemmerer S, Berry JA. A biochemical model of photosynthetic CO₂ assimilation in leaves of C₃ species. *Planta* 1980;149:78–90.
- [21] Farquhar GD, Sharkey TD. Stomatal conductance and photosynthesis. *Ann Rev Plant Physiol* 1982;33:317–45.
- [22] Fassnach KS, Gower ST. Comparison of the litterfall and forest floor organic matter and nitrogen dynamics of upland forest ecosystems in north central Wisconsin. *Biogeochemistry* 1999;43:265–84.
- [23] Fassnacht KS, Gower ST, MacKenzie MD, Nordheim EV, Lillesand TM. Estimating the leaf area of north central Wisconsin forests using the Landsat Thematic Mapper. *Remote Sens Environ* 1997;61:209–22.
- [24] Foley JA, Prentice IC, Ramankutty N, Levis S, Pollard D, Sitch S, Haxeltine A. An integrated biosphere model of land surface processes, terrestrial carbon balance, and vegetation dynamics. *Global Biogeochem Cyc* 1996;10(4):603–28.
- [25] Foley JA, Levis S, Costa MH, Cramer W, Pollard D. Incorporating dynamic vegetation cover within global climate models. *Ecol Appl* 2000;10(6):1620–32.
- [26] Franks SW, Beven KJ. Estimation of evapotranspiration at the landscape scale: a fuzzy disaggregation approach. *Water Resour Res* 1997;33(12):2929–38.
- [27] Franks SW, Beven KJ. Conditioning a multiple-patch SVAT model using uncertain timespace estimates of latent heat fluxes as inferred from remotely sensed data. *Water Resour Res* 1999;35(9):2751–61.
- [28] Gardner WR. Some steady-state solutions of the unsaturated moisture flow equation with application to evaporation from a water table. *Soil Sci* 1958;85:228–32.
- [29] Goudriaan J. *Crop micrometeorology: a simulation study*. Simulation Monographs. Wageningen; 1977.
- [30] Granier A. Evaluation of transpiration in a Douglas fir stand by means of sap flow measurements. *Tree Physiol* 1987;3:309–20.
- [31] Gupta HV, Sorooshian S, Yapo PO. Towards improved calibration of hydrologic models: multiple and non-commensurable measures of information. *Water Resour Res* 1998;34(4):751–63.
- [32] Hartley RVL. Transmission of information. *Bell Syst Tech J* 1928;7(3):535–63.
- [33] Higashi M, Klir GJ. On measures of fuzziness and fuzzy complements. *Int J Gen Syst* 1982;8(3):169–80.
- [34] Jarvis PG. The interpretation of the variations in leaf water potential and stomatal conductance found in canopies in the field. *Philos Trans Roy Soc Lond Ser B* 1976;273:593–610.
- [35] Jarvis PG. Stomatal response to water stress in conifers. In: Turner NC, Kramer PJ, editors. *Adaptation of Plants to Water and High Temperature Stress*. New York: John Wiley and Sons; 1980. p. 105–22.
- [36] Jarvis PG, McNaughton KG. Stomatal control of transpiration: scaling up from leaf to region. *Adv Ecol Res* 1986;15:1–49.
- [37] Kelliher FM, Leuning R, Schulze E-D. Evaporation and canopy characteristics of coniferous forests and grasslands. *Oecologia* 1993;95:153–63.
- [38] Kelliher FM, Leuning R, Raupach MR, Schulze E-D. Maximum conductances for evaporation from global vegetation types. *Agri Forest Meteorol* 1995;73:1–16.
- [39] Klepper O, Scholten H, Van De Kamer JPG. Prediction uncertainty in an ecological model of the Oosterschelde Estuary. *J Forecast* 1991;10:191–209.
- [40] Klir GJ, Wierman MJ. *Uncertainty-based information: elements of generalized information theory*. Heidelberg: Physica-Verlag; 1998.
- [41] Kuczera G, Parent E. Monte Carlo assessment of parameter uncertainty in conceptual catchment models: the Metropolis algorithm. *J Hydrol* 1998;211:69–85.
- [42] Leuning R, Kelliher FM, De Pury DGG, Schulze E-D. Leaf nitrogen, photosynthesis, conductance and transpiration: scaling from leaves to canopies. *Plant Cell Environ* 1995;18:1183–200.
- [43] Lohammar T, Larsson S, Linder S, Falk SO. FAST-simulation models of gaseous exchange in Scots pine. In: Persson T, editor. *Structure and function of northern coniferous forests—an ecosystem study*, 32. *Ecological Bulletin*; 1980. p. 505–23.
- [44] Mackay DS. Evaluation of hydrologic equilibrium in a mountainous watershed: incorporating forest canopy spatial adjustment to soil biogeochemical processes. *Adv Water Resour* 2001;24(9–10):1211–27.
- [45] Mackay DS, Ahl DE, Ewers BE, Gower ST, Burrows SN, Samanta S, Davis KJ. Effects of aggregated classifications of forest composition on estimates of evapotranspiration in a northern Wisconsin forest. *Global Change Biol* 2002;8(12):1253–65.
- [46] Mackay DS, Band LE. Forest ecosystem processes at the watershed scale: dynamic coupling of distributed hydrology and canopy growth. *Hydrol Process* 1997;11:1197–217.
- [47] Magnani F, Leonardi S, Tognetti R, Grace J, Borghetti M. Modelling the surface conductance of a broad-leaf canopy: effects of partial decoupling from the atmosphere. *Plant Cell Environ* 1998;21:867–79.
- [48] McNaughton KG, Jarvis PG. Effects of spatial scale on stomatal control of transpiration. *Agri Forest Meteorol* 1991;54:279–301.
- [49] Monteith JL. *Evaporation and environment*. In: *Symposium of the Society for Experimental Biology*. New York: Cambridge University Press; 19th. p. 205–33.
- [50] Monteith JL. A reinterpretation of stomatal response to humidity. *Plant Cell Environ* 1995;18:357–64.
- [51] Monteith JL, Unsworth MH. *Principles of environmental physics*. 2nd ed. New York: Edward Arnold; 1990.
- [52] Nemani RR, Running SW. Estimation of regional surface resistance to evapotranspiration from NDVI and thermal-IR ANHRR data. *J Appl Meteorol* 1989;28(4):276–84.
- [53] Oren R, Sperry JS, Katul GG, Pataki DE, Ewers BE, Phillips N, Schafer KVR. Survey and synthesis of intra- and interspecific variation in stomatal sensitivity to vapour pressure deficit. *Plant Cell Environ* 1999;22:1515–26.
- [54] Pataki DE, Oren R, Smith WK. Sap flux of co-occurring species in a western subalpine forest during seasonal soil drought. *Ecology* 2000;81(9):2557–66.
- [55] Phillips N, Oren R. A comparison of daily representations of canopy conductance based on two conditional time-averaging methods. *Ann Sci For* 1998;55:191–216.

- [56] Pierce LL, Congalton RG. A methodology for mapping forest latent heat flux densities using remote sensing. *Remote Sens Environ* 1988;24:405–18.
- [57] Running SW, Coughlan JC. A general model of forest ecosystem processes for regional applications I. Hydrologic balance, carbon gas exchange and primary production processes. *Ecol Model* 1988;42:125–54.
- [58] Running SW, Gower ST. FOREST-BGC, a general model of forest ecosystem processes for regional applications. II. Dynamic carbon allocation and nitrogen budgets. *Tree Physiol* 1991;9:147–60.
- [59] Running SW, Hunt Jr ER. Generalization of a forest ecosystem process model for other biomes, BIOME-BGC, and application for global scale models. In: Ehleringer JR, Field CB, editors. *Scaling Physiological Processes: Leaf to Globe*. San Diego, CA: Academic Press; 1993. p. 141–58.
- [60] Running SW, Loveland TR, Pierce LL, Nemani RR, Hunt Jr ER. A remote sensing based vegetation classification logic for global land cover analysis. *Remote Sens Environ* 1995;51:39–58.
- [61] Saliendra NZ, Sperry JS, Comstock JP. Influence of leaf water status on stomatal response to humidity, hydraulic conductance, and soil drought in *Betula occidentalis*. *Planta* 1995;196:357–66.
- [62] Samanta S, Mackay DS. Flexible automated parameterization of hydrologic models using fuzzy logic. *Water Resour Res*, in press.
- [63] Sellers PJ, Dickinson RE, Randall DA, et al. Modeling the exchange of energy, water, and carbon between continents and the atmosphere. *Science* 1997;275:502–9.
- [64] Sellers PJ, Los SO, Tucker CJ, Justice CO, Dazlich DA, Collatz GJ, Randall DA. A revised land surface parameterization (SiB2) for atmospheric GCMs. Part II: The generation of global fields of terrestrial biophysical parameters from satellite data. *J Climate* 1996;9:676–705.
- [65] Sivapalan M, Beven K, Wood EF. On hydrologic similarity 2. A scaled model of storm runoff production. *Water Resour Res* 1987;23:2266–78.
- [66] Sorooshian S, Gupta VK. Automatic calibration of conceptual rainfall-runoff models: the question of parameter observability and uniqueness. *Water Resour Res* 1983;19(1):251–9.
- [67] Spear RC, Hornberger GM. Eutrophication in Peel Inlet—II identification of critical uncertainty via generalized sensitivity analysis. *Water Resour Res* 1990;14:43–9.
- [68] Sperry JS, Adler JR, Campbell GS, Comstock JS. Hydraulic limitation of a flux and pressure in the soil-plant continuum: results from a model. *Plant Cell Environ* 1998;21:347–59.
- [69] Tyree MT, Ewers FE. The hydraulic architecture of trees and other woody plants. *New Phytol* 1991;119:345–60.
- [70] Tyree MT, Sperry JS. Do woody plants operate near the point of catastrophic xylem dysfunction caused by dynamic water stress? Answers from a model. *Plant Physiol* 1988;88:574–80.
- [71] Van Stratten G, Keesman KJ. Uncertainty propagation and speculation in projective forecasts of environmental change: a lake-eutrophication example. *J Forecast* 1991;10:163–90.
- [72] Vertessy RA, Hatton TJ, Benyon RG, Dawes WR. Long-term growth and water balance predictions for a mountain ash (*Eucalyptus regnans*) for catchment subject to clearfelling and regeneration. *Tree Physiol* 1996;16:221–32.
- [73] Wigmosta MS, Vail LW, Lettenmaier DP. A distributed hydrology-vegetation model for complex terrain. *Water Resour Res* 1994;30(6):1665–79.
- [74] Wullschlegel SD. Biochemical limitations to carbon assimilation in C_3 plants—A retrospective analysis of the A/C_i curves from 109 species. *J Exp Botany* 1993;44(262):907–20.
- [75] Yong JWH, Wong SC, Farquhar GD. Stomatal response to changes in vapour pressure difference between leaf and air. *Plant Cell Environ* 1997;20:1213–6.
- [76] Zadeh LA. Fuzzy sets. *Informat Contr* 1965;8(3):338–53.
- [77] Zadeh LA. Fuzzy sets as a basis for a theory of possibilities. *Int J Fuzzy Sets Syst* 1978;1(1):3–28.
- [78] Zeng X, Dickinson RE, Walker A, Shaikh M, DeFries RS, Qi J. Derivation and evaluation of global 1-km fractional vegetation cover data for land modeling. *J Appl Meteorol* 2000;39:826–39.